Drag Coefficients with Fetch-Limited Wind Waves*

WEIQI LIN,+ LAWRENCE P. SANFORD, AND STEVEN E. SUTTLES

Horn Point Laboratory, University of Maryland Center for Environmental Science, Cambridge, Maryland

RICHARD VALIGURA#

Air Resource Laboratory, National Oceanic and Atmospheric Administration, Silver Spring, Maryland

(Manuscript received 10 July 2001, in final form 9 April 2002)

ABSTRACT

Air–sea fluxes of momentum and heat were measured simultaneously with surface wind waves and near-surface currents in mid Chesapeake Bay during summer 1998 under low wind conditions. The data were collected using a Gill sonic anemometer and a Sontek Acoustic Doppler Velocimeter with a pressure sensor mounted on a temporary fixed tower in 8.8 m of water. The analyzed data show that the neutral drag coefficients depend upon both wind speed and wave age. They are better correlated to wave age than to wind speed. Data scatter is significantly larger in low winds than in high winds. Under light winds, the neutral drag coefficients increase with decreasing wind speed and have values much higher than those for relatively higher wind speeds. At higher wind speeds, neutral drag coefficients increase with increasing wind speed. Regardless of wind speed, neutral drag coefficients always decrease with increasing wave age. Neutral drag coefficients are lower than the results of similar field studies when fit to wind speed alone, but they statistically agree with other studies if they are fit to wave age. The momentum transfer mechanism is investigated using a parametric wave model with a sea-state-dependent form drag and a reference system moving with the waves. The relationship between modeled drag coefficient and modeled wave age agrees well with the relationship derived from the data.

1. Introduction

Through transfer of momentum and sensible and latent heat, the turbulent atmospheric and oceanic boundary layers couple with each other across the wavy interface. This complex set of interactions is often expressed in terms of a drag coefficient (C_d) or an aerodynamic surface roughness (z_0). Because of its central role in understanding and modeling air–sea interaction processes, C_d or z_0 has been studied extensively from observations and numerical models in the past few decades. One important issue has been and continues to be the role of surface gravity waves in determining C_d or z_0.

Several field experiments have reported evidence of wave age dependence in C_d or z_0, for example, the Marine Remote Sensing (MARSEN) program (Geernaert et al. 1987), the Humidity Exchange over the Sea (HEXOS) program in the North Sea, the HEXOS Main Experiment (HEXMAX) off the Dutch coast (Smith et al. 1992), and the Risø Air Sea Experiment (RASEX) in Denmark (Mahrt et al. 1996; Vickers and Mahrt 1997). Other literatures (e.g., Kitaigorodskii 1968, 1970; Donelan et al. 1985; Donelan 1990; Merzi and Graf 1985; Toba et al. 1990) also suggested that wave age is an important parameter for determining C_d or z_0. Most of these studies are based on data collected in fetch-limited conditions either in coastal waters or lakes. For open ocean data, however, a clear wave age dependence has not been reported (Dobson et al. 1994; Rieder 1997; Taylor and Yelland 2001). Therefore, a few studies (Smith and Banke 1975; Garratt 1977; Smith 1980; Large and Pond 1981) concluded that C_d or z_0 depends on wind speed only.

Under steady state and horizontally homogeneous conditions, the wind profile in the atmospheric boundary layer can be described by the Monin–Obukhov (1954) similarity theory. The vertical wind profile is

$$\frac{U_z}{u_*} = \frac{1}{\kappa}\left[\ln\left(\frac{z}{z_0}\right) - \psi_m\left(\frac{z}{L}\right)\right], \tag{1}$$

where U_z is the wind speed measured at anemometer

* University of Maryland Center for Environmental Science Publication Number 3577.

+ Current affiliation: Oceanography Division, Naval Research Laboratory, Stennis Space Center, Mississippi.

Current affiliation: Integrated Forest Management, LLC, Sun Prairie, Wisconsin.

Corresponding author address: Dr. Lawrence P. Sanford, Horn Point Laboratory, University of Maryland Center for Environmental Science, P.O. Box 775, Cambridge, MD 21613.
E-mail: lsanford@hpl.umces.edu

height z, u_* is the surface wind friction velocity and is given by $(\tau/\rho_a)^{1/2}$, τ is wind stress, κ is the von Kármán constant ($=0.41$ in this study), and L is the Monin–Obukhov stability length. It can be estimated by

$$L = \frac{u_*^2\theta\left[\ln\left(\frac{z}{z_0}\right) - \psi_m\left(\frac{z}{L}\right)\right]}{\kappa^2 g(\theta_a - \theta_s)}, \quad (2)$$

where g is the gravity, θ is the mean potential temperature in the boundary layer; θ_a is the air potential temperature and θ_s is the sea surface potential temperature. Here ψ_m (z/L) has been determined empirically (e.g., Liu et al. 1979; Large and Pond 1982; Panofsky and Dutton 1984; Erickson 1993; Ataktürk and Katsaros 1999). In the stable case ($L > 0$),

$$\psi_m\left(\frac{z}{L}\right) = -7\frac{z}{L}, \quad (3)$$

and in the unstable case ($L < 0$),

$$\psi_m\left(\frac{z}{L}\right) = 2\ln\left(\frac{1+x}{2}\right) + \ln\left(\frac{1+x^2}{2}\right) - 2\tan^{-1}(x) + \frac{\pi}{2}, \quad (4)$$

where $x = (1 - 16z/L)^{1/4}$. The drag coefficient is defined as $C_d = (u_*/U_{n10})^2$ and a unique relationship between C_d and z_0 can be derived as $C_d = [\kappa/\ln(z/z_0)]^2$ under neutrally stratified conditions.

Equation (1) is developed over land and is valid only under stationary and horizontally homogeneous conditions. Also, it cannot be applied very close to the surface where molecular transport is dominant and turbulence is suppressed. When applied in a marine environment, the over water atmospheric boundary layer must also meet the stationary and horizontally homogeneous conditions so that the surface layer can be treated as a constant stress layer. Under light wind conditions, the flow is aerodynamically smooth and viscous stresses dominate the momentum flux from air to the water surface. The surface roughness is parameterized with the friction velocity and the kinematic viscosity of air (e.g., Smith 1980; Large and Pond 1981; Donelan 1990; Banner et al. 1999):

$$z_0 = 0.11\frac{\nu_a}{u_*}, \quad (5)$$

where $\nu_a = 1.4 \times 10^{-5}$ m^2 s^{-1} is the kinematic viscosity of air. The speed limit for a smooth flow condition is given by $u_* < 2(\nu_a g)^{1/3}$ (Donelan 1990) and can be estimated as $u_* = 0.103$ m s^{-1}, or $U_{n10} \approx 3.0$ m s^{-1}. The thickness of the viscous sublayer decreases with the increasing friction velocity. As wind speeds increase, the friction velocity increases and a windsea develops. A growing fraction of the momentum flux from air to the sea surface occurs as wave form drag. The surface makes a transition from a relatively smooth flow to a rough state with the waves penetrating through the viscous sublayer and interacting with the air flow. The surface roughness length increases and the airflow becomes aerodynamically rougher. For fully developed waves, Charnock (1955) proposed that z_0 could be given as

$$z_0 = \alpha\frac{u_*^2}{g}, \quad (6)$$

where $\alpha = 0.012$ (Charnock 1958) is the Charnock constant. The values of α derived from data in the open ocean with well-developed waves do not agree with those obtained with fetch limited waves. For example, Smith (1980, 1988) and Large and Pond (1981) have shown that $\alpha = 0.011$ best describes the dependence of C_d on wind speed observed over deep open ocean conditions. But applications to the datasets obtained in coastal waters or lakes with presumably less mature waves resulted in higher values of α, for example, $\alpha = 0.0145$ by Garratt (1977) and $\alpha = 0.018$ by Wu (1980).

Most of the field experiments over the past have established a statistically significant dependence of C_d on U_{n10}. The general form of this linear regression can be expressed as

$$C_d = (a + bU_{n10}) \times 10^{-3}, \quad (7)$$

where a and b are coefficients determined by the data. In MARSEN, $a = 8.47 \times 10^{-2}$ and $b = 0.577$ (Geernaert et al. 1987); in HEXMAX, $a = 9.1 \times 10^{-2}$ and $b = 0.50$ (Smith et al. 1992); in RASEX, $a = 6.7 \times 10^{-2}$ and $b = 0.75$ for $U_{n10} > 4$ m s^{-1} (Vickers and Mahrt 1997); and in Surface Wave Dynamics Experiment (SWADE), $a = 7.0 \times 10^{-2}$ and $b = 0.6$ for 6 m s^{-1} $< U_{n10} <$ 14 m s^{-1} (Drennan et al. 1999). Banner et al. (1999) also selected quite a few observational results and showed a surprising large scatter among them. The review by Wu (1980) and Geernaert (1990) listed many different values of the coefficients for different observations.

It is clear that the variability of C_d not explained by U_{n10} is substantial. The surface waves must play a role in air–sea momentum fluxes. The wave form drag changes with wave age and in a fully developed wave field, the dominant waves traveling at phase speeds close to the wind velocity receive little momentum from the air (Dobson and Elliott 1978; Snyder et al. 1981; Hsiao and Shemdin 1983; Hasselmann et al. 1986). Steward (1974) recommended that a sea-state-dependent Charnock constant be used:

$$\alpha = \frac{gz_0}{u_*^2} = f\left(\frac{C_p}{u_*}\right), \quad (8)$$

where C_p is the phase velocity of the waves at the spectral peak. The form of the function in the right hand side of Eq. (8) can be different. A widely used function is

$$C_d = A\left(\frac{C_p}{u_*}\right)^B, \tag{9}$$

where A and B are coefficients determined by the data. In MARSEN, $A = 1.48 \times 10^{-2}$ and $B = -0.738$ when long period swells are not included; in HEXMAX, $A = 0.43$ and $B = -0.961$; in RASEX, $A = 7.1 \times 10^{-3}$ and $B = -2/3$. However, Eqs. (8) and (9) may have a self-correlation problem if other variables, like C_p or u_*, have a limited range (Perrie and Toulany 1990; Smith et al. 1992).

Avoiding these problems, Donelan (1990) proposed a relationship between z_0, H_s, and wave age C_p/U_{n10} (rather than C_p/u_*) for fully rough flow,

$$\frac{z_0}{H_s} = 1.38 \times 10^{-4}\left(\frac{C_p}{U_{n10}}\right)^{-2.66}, \tag{10}$$

based on data collected nearshore in Lake Ontario, Canada. Equation (10) is derived from data with fetch-limited waves and absence of swells or mixed seas. Similarly, Hsu (1974) suggested that Charnock constant is a function of wave steepness. Most recently, Taylor and Yelland (2001) combined the HEXMAX, RASEX, and Lake Ontario datasets (Anctil and Donelan 1996) and proposed that z_0 be parameterized by the height and steepness of the waves,

$$\frac{z_0}{H_s} = 1200\left(\frac{H_s}{L_p}\right)^{4.5}, \tag{11}$$

where L_p is the wave length at the spectral peak.

Despite a large number of field studies, controversy remains over the nature of the relationship among wind, sea state, and drag. A comprehensive reference and background knowledge on this subject have been given in Donelan (1990), Geernaert (1990), and more recently by Banner et al. (1999). In this paper, we present new data from an atmospheric boundary layer and surface wave study under almost purely fetch-limited conditions, with fetches ranging from a few to tens of kilometers (section 2). We present relationships between C_d, U_{n10} and C_p/u_* derived from these data and compare the results with other observations (section 3). We also explore the mechanism underlying the results using a parametric wave model with a wave-age-dependent form drag and a wave-following reference frame (section 4). The model is a straightforward extension of the wave model developed by Donelan (1977). Finally, we summarize and conclude our study in section 5.

2. Experimental design and data analysis

a. Experiment layout

The field data used in this study were collected in the middle reaches of Chesapeake Bay (CB). The bay is a semienclosed basin and the largest estuary in the United States and stretches 320 km from the Susquehanna River to the Atlantic Ocean. It varies from 7 to 50 km in width and its average water depth is about 8.5 m. Surface waves in the mid CB are dominated by fetch-limited windseas (Sanford 1994; Lin et al. 1998; Lin 2000). Fetch varies strongly as a function of wind direction and location. Swell generated in the Atlantic Ocean can only affect the wave climate in the southern bay (Boon 1998). The swell energy is dissipated to undetectable levels by the time it reaches the mid CB. Thus, field experiments conducted in mid CB cover a wide range of wave ages under almost entirely fetch-limited conditions.

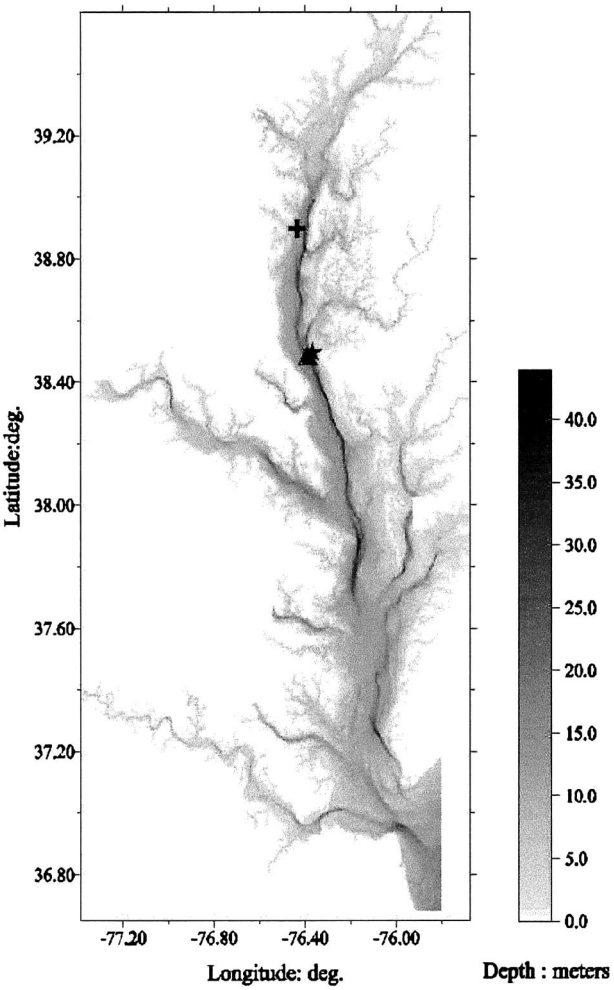

FIG. 1. The Chesapeake Bay bathymetry and the tower and buoy locations for the field experiment: ★ tower location, ▲ CBOS buoy, and + Thomas Point Light tower.

The field experiment was carried out from 19 to 28 July 1998. A temporary fixed tower was deployed at 38°29′41″N, 76°22′11″W on a shallow shelf adjacent to the deep center channel, approximately 3 km from the eastern shore and 10 km from the western shore (Fig. 1). The water depth at the tower site was 8.8 m with a mean tidal range of approximately 0.6 m. The tower height was 11 m. On top of the tower, a rectangular

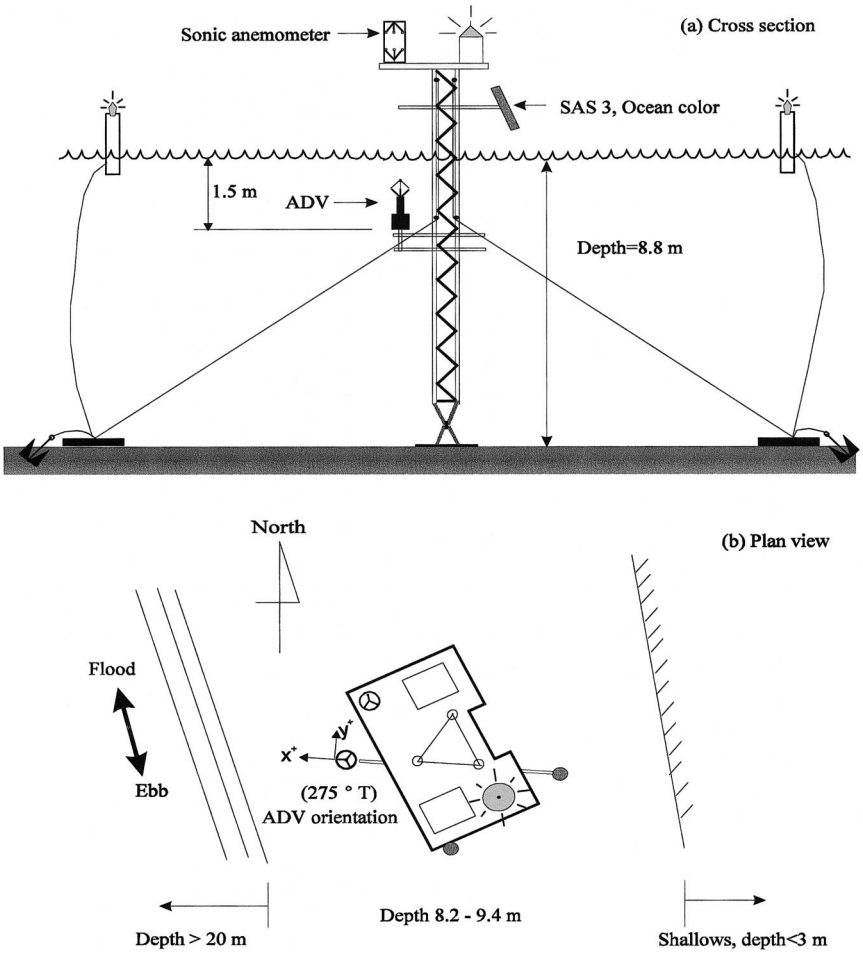

FIG. 2. Layout of the temporary fixed tower for the experiment: (a) cross section and (b) plan view.

platform (1.8×1.2 m^2) was mounted for deploying a navigation safety light, a Gill sonic anemometer and an infrared hygrometer (IRGA). The sonic anemometer and hygrometer were centered at 0.8 m above the platform and 3.8 m above mean water level. Surface wind waves and near-surface water velocities were measured simultaneously using an acoustic Doppler velocimeter (ADV) and pressure sensor mounted 1.5 m below mean water level. The layout of the tower is shown in Fig. 2. The air–sea flux data were recorded using a battery operated data acquisition system, the memory of which had to be manually downloaded to a laptop computer at regular intervals. This limited the amount of data collected during the 10-day experimental period because of practical constraints on servicing the system.

A buoy of the Chesapeake Bay Observing System (CBOS) was located about 2 km southwest of the tower at 38°28′24″N, 76°22′48″W (Fig. 1). The buoy recorded wind speed and direction, water and air temperatures, relatively humidity, barometric pressure, salinity, and current speed and direction continuously over the duration of the experiment. A wind sensor at $z = 3.5$ m recorded average wind speed and direction every half hour. Surface currents were measured 2.4 m below the water surface. Barometric pressure data from the buoy were utilized to correct the underwater pressure data collected at the tower. The buoy surface water temperature (T_w) was used for atmospheric stability corrections. The surface current data were used to correct surface wind speed.

b. Air–sea fluxes

The Gill sonic anemometer and IRGA package on the fixed tower recorded the turbulent Reynold stress $\rho_a\langle u'w'\rangle$, wind speed and direction, air temperature (T_a), and heat and moisture fluxes. The package sampled at 10 Hz for 30-min intervals, collecting a total of 18 000 data points during each interval. It resolved the wind into three orthogonal components, u along the direction of the mean wind, v horizontally transverse to it, and w in the vertical. Eddy fluxes of momentum, heat, and moisture were calculated by combining the hygrometer measurements of water vapor and T_a with the sonic ane-

mometer measurements, using the micrometeorological methods of McMillan (1987) and Baldocchi et al. (1988). Momentum flux from air to water was calculated as

$$u_* = (\overline{u'w'})^{1/2}. \quad (12)$$

Eddy flux of sensible heat, H, was computed as

$$H = \rho_a c_a \overline{w'T'}, \quad (13)$$

where c_a is the specific heat of air at constant pressure. Latent heat flux, LE, was calculated as

$$\mathrm{LE} = \rho_a L_{\mathrm{vap}} \overline{w'q'}, \quad (14)$$

where LE is the evaporation rate, L_{vap} is the latent heat of vaporization of water, and q is the specific humidity. Here L can be calculated as

$$L = \frac{\rho_a c_a u_*^3 \theta}{\kappa g(H + \mathrm{LE}/14)}. \quad (15)$$

Wind speeds measured at the tower were converted to U_{n10} using the calculated stability length from the flux measurements; U_{n10} was corrected with surface currents by

$$U_{n10} = |\mathbf{u}'_{n10} - \mathbf{u}_c|, \quad (16)$$

where $\mathbf{u}'_{n10}$ is the neutral 10-m wind velocity before correction and $\mathbf{u}_c$ is the surface current.

We used 30 min as the averaging time both for sampling and calculating the covariances. Under stationary and horizontally homogenous conditions, the averaging time used to define the perturbations can be as small as 5 min to capture most of the stress value. But the flux average time should be much longer. Pierson (1983) suggested an averaging time of 20 min for air–sea turbulent studies. However, Donelan (1990) found that a 20-min averaging time produced rather inaccurate stress estimates, and the accuracy was particularly poor in light winds at $z < 10$ m. Banner et al. (1999) pointed out that data must be measured over sufficiently large time and space scales to capture all scales of variability for the eddy correction technique. The 30-min averaging time at $z = 3.8$ m was chosen to reduce sampling errors in the data analysis, especially since the dataset contained about 25% data points in light winds. This is also long enough to include all the significant spectral frequency contributions from surface waves (Geernaert et al. 1988).

c. Surface waves

Surface waves were measured by a 5-MHz Sontek ADV with a pressure sensor. The instrument recorded pressure and velocity components. Both the ADV and the pressure sensor were sampled at 4 Hz for 450 s, with a new burst recorded every 30 min. Water level variations and directional wave spectra were calculated from the velocity and pressure data. A correction for changes in atmospheric pressure was first applied to the subsurface pressure record using barometric pressure data from the buoy. A modified version of WavePro, a software package developed by Woods Hole Instrument Systems, Ltd., was used to carry out the directional wave spectral analysis. WavePro uses the directional spectral analysis technique of Longuet-Higgins (1963) to calculate directional wave spectra. The modification made was that the subsurface pressure and velocity record were transferred to surface elevation using a semi-empirical transfer function in the time domain (Nielsen 1989), instead of the standard linear transformation that is made after the signal is converted to the frequency domain. Nielsen's procedure was used because linear wave theory is not expected to perform well at high frequencies when calculating surface elevation from subsurface pressure, largely because of instrument noise. In this dataset, the high frequency information up to the cutoff Nyquist frequency is important and needs to be retained. Nielsen's function was designed by direct physical reasoning supplemented as appropriate with empirical quantification in the time domain. Significant wave heights, peak periods and mean wave directions were derived from the directional wave spectra.

The measured wind, surface wave, and air–sea temperature data are shown in Fig. 3. The CBOS raw wind vectors are plotted in Fig. 3. The tower wind data are not shown because they were not a continuous time series. The available air–sea flux data are shown in Fig. 3 by dots under the raw wind vectors.

d. The frontal systems

During the summer season, frontal systems frequently pass through the study area. We inspected the NOAA Daily Weather Map (weekly series) for the period of 19–28 July 1998 when the tower experiment was conducted. A day before the tower was deployed, there was a strong cold front passing through the area. On 19 July, this front became stationary and stalled far south of the area, near the bay mouth. It moved away the next day. The wind and T_a recorded from the buoy did not show another clear frontal passage until 24 July when a strong cold frontal system formed. Both wind and T_a in Fig. 3 showed the influence of this front with wind direction veering from southwest to northwest and T_a dropping significantly. On 25 July, a low pressure center became established east of Virginia and the frontal system became stationary south of CB for the next three days until 29 July.

e. Data selection

The succession of frontal systems during the field experiment made the study area less stationary and spatially homogenous and might have led to errors in the air–sea flux measurements (Ataktürk and Katsaros 1999). Therefore, a careful selection of the measured data was carried out to reduce the influence of rapid spatial and temporal variability. The potential influence

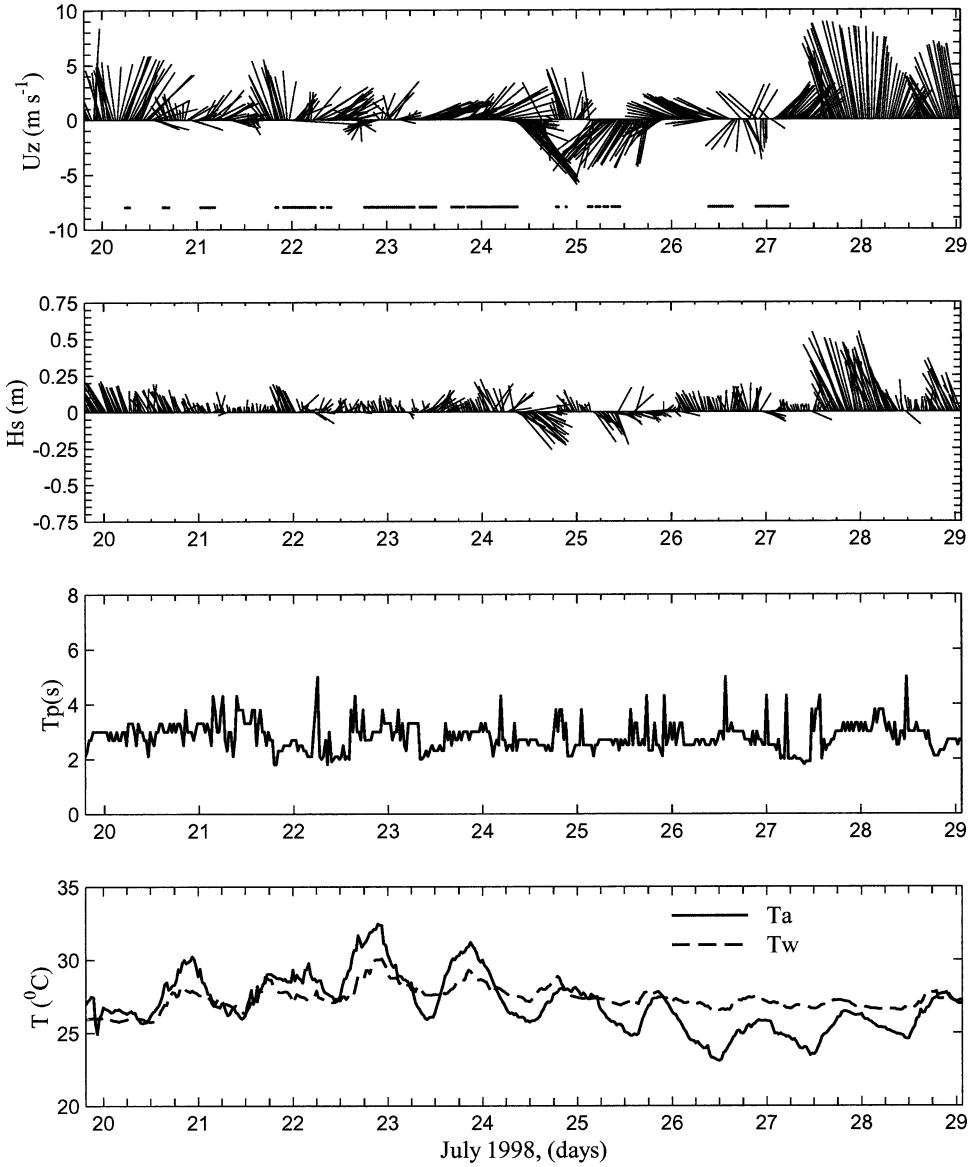

FIG. 3. The time series of (a) measured wind speeds and directions, (b) significant wave heights and mean wave directions, (c) peak wave periods, and (d) air and sea temperatures for the tower experiment from 19 to 28 Jul 1998. The lengths of the vectors are used to show the magnitude of the wind speed or significant wave height. The pointing directions of the vectors show wind directions or mean wave directions. The wind data in (a) are from CBOS raw wind data with the available air–sea flux data shown by dots under the raw wind vectors.

of large-scale flows on air–sea momentum fluxes was recently addressed in the Southern Ocean Waves Experiment (SOWEX; Banner et al. 1999; Chen et al. 2001), but this topic is beyond the scope of the present study.

In order to focus on the role of surface waves on the air–sea momentum fluxes, we carefully selected the available air–sea flux data to meet the stationarity and horizontal homogeneity required by the Monin–Obukhov similarity theory. If the wind speed was extremely low (<1 m s^{-1}) or there were rapid changes in wind direction and speed, that half-hour's data were not used. We also compared wind data measured by the sonic anemometer at the tower site with those simultaneously measured at the CBOS buoy. If the difference in wind speed was more than 1 m s^{-1} or the difference in the wind direction was greater than 45°, that half hour's data were not used either. Because similarity theory is considered valid only if stability parameters (z/L) are in the range of $[-1, 1]$ (Valigura 1995), both extremely stable or unstable conditions with $z/L > 1$ or $z/L < -1$ were further excluded from the analysis since in these

TABLE 1. The neutral drag coefficients for different wind speed bins from data and model.

	Data				Model			
U_{n10} (m s^{-1})	Mean C_d ($\times 10^{-3}$)	Std dev ($\times 10^{-3}$)	Std error ($\times 10^{-3}$)	N	Mean C_d ($\times 10^{-3}$)	Std dev ($\times 10^{-3}$)	Std error ($\times 10^{-3}$)	N
0.5–1.5	2.084	0.941	0.544	3	1.559	1.517	0.323	22
1.5–2.5	1.683	0.791	0.299	7	0.927	0.418	0.082	26
2.5–3.5	1.022	0.591	0.178	11	0.869	0.092	0.018	27
3.5–4.5	0.857	0.385	0.136	8	0.961	0.114	0.018	41
4.5–5.5	0.916	0.270	0.044	38	1.017	0.098	0.014	46
5.5–6.5	0.935	0.189	0.031	38	1.089	0.100	0.020	26
6.5–7.5	1.005	0.169	0.047	13	1.133	0.074	0.021	12
7.5–8.5	1.009	0.182	0.064	8	1.231	0.117	0.037	10
8.5–9.5	1.047	0.108	0.036	9	1.311	0.086	0.027	10

cases the turbulence is either severely damped or dominated by buoyancy production. Furthermore, data from wind, wave, and current directions that would have placed either sensor in the wake of the tower were discarded to eliminate systematic errors due to wind or current shadowing. A total of 17 data points were eliminated using these criteria, all of them with U_{n10} less than 4 m s^{-1}. We had 135 data points left for analysis relative to wind speeds. Among them, 34 (25%) data points had wind speed less than 4 m s^{-1} and 101 (75%) of them had wind speed greater than 4 m s^{-1}.

Wave data were selected independently from the wind data. The analyzed peak wave periods had anomalies when significant wave height was very low because the response of the pressure sensor was not very reliable for high frequency waves. Therefore, all data points with significant wave heights less than 10 cm were eliminated. A total of 119 data points with both air–sea flux data and wave data were available for further analysis.

3. Results and discussion

The 135 data points for wind speed analysis were equally grouped into nine 1 m s^{-1} wind speed bins, from 0.5 to 1.5 m s^{-1}, . . . , 8.5 to 9.5 m s^{-1}. The mean values of C_d and U_{n10} were calculated for each bin. The standard error, defined as the sample standard deviation divided by the square root of the number of samples, was also calculated. The mean C_d, standard deviation, standard error, and the sample number for each wind speed bin are listed in Table 1. Also, the mean C_d with standard error bars are plotted against U_{n10} in Fig. 4. Both Table 1 and Fig. 4 show that C_d increases with decreasing wind speed under light winds ($U_{n10} < 4$ m s^{-1}) and has values much higher than for relatively higher wind speeds (4 m s^{-1} $< U_{n10} <$ 10 m s^{-1}); C_d increases with increasing wind speed for $U_{n10} > 4$ m s^{-1}. The standard errors for low wind speeds are significantly larger than those for higher wind speeds.

Across the entire range of smooth, transitional, and rough turbulent flow C_d can be defined by z_0, as the sum of Eq. (5) and (6), such that

$$z_0 = 0.11\frac{\nu_a}{u_*} + \alpha\frac{u_*^2}{g}. \quad (17)$$

Using Eq. (17), the calculated C_d for $\alpha = 0.012$ is plotted in Fig. 4 for comparison to our data. The data are approximately 90% higher than this relationship at the lowest wind speeds. Thus, an increase in apparent roughness due to the growth of the viscous sublayer does not explain the magnitude of the C_d increase that we observed at low wind speeds. On the other hand, our data are about 20% less than the Charnock relationship for $U_{n10} > 4$ m s^{-1}. We also calculated C_d corresponding to the wave-age-dependent surface roughness in Eq. (10) proposed by Donelan (1990). We used our observed values of H_s, T_p, and U_{n10} for these calculations and plotted the results in Fig. 4. They show less scatter than our data, are generally larger than our data for $U_{n10} > 4$ m s^{-1}, agree with the Charnock formulation for 4 m s^{-1} $< U_{n10} <$ 7 m s^{-1}, and are larger than the Charnock relationship for $U_{n10} > 7$ m s^{-1}.

In order to compare our observed dependence of C_d on U_{n10} with other studies, data points with $U_{n10} > 4$ m s^{-1} were linearly regressed as in Eq. (7) using $N = 101$ samples. A best fit is found to be

$$C_d = (0.0467U_{n10} + 0.643) \times 10^{-3}. \quad (18)$$

The correlation coefficient was quite low ($r = 0.273$). The linear regression in Eq. (18) is plotted in Fig. 5 for comparison with results from MARSEN, HEXMAX, RASEX, and SWADE. The Charnock relationship is also shown for comparison. Our data show a lower C_d than all of the other observations when C_d is considered as a function of U_{n10} alone. This discrepancy in comparison with other results and the large scatter imply that another source of variability, very possibly the wave age, may play an important role.

To test the dependence of the drag coefficient on wave age, the 119 pairs of C_d and C_p/u_* were fit to an equation of the form of Eq. (9). Our data gave a best fit of $A = 6.28 \times 10^{-3}$ and $B = -0.578$, with a correlation coefficient of $r = 0.64$, significantly higher than that for the U_{n10} fit. The standard error for A was 1.105×10^{-3} and for B was 0.0589. The regression is plotted in Fig.

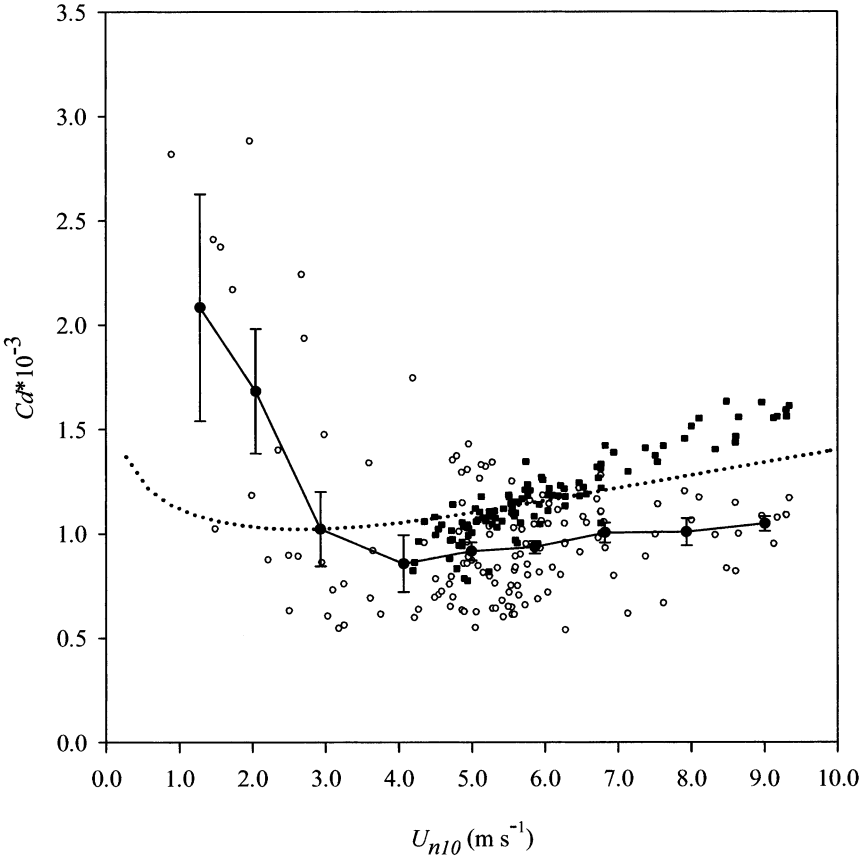

FIG. 4. Comparison of observed mean neutral drag coefficients for nine 1 m s^{-1} different wind speed bins with those calculated from Eq. (17) (dotted line) and Eq. (10) (solid squares). The data points are shown by open circles. Error bars represent the standard error for each wind speed bin.

6 for comparison with MARSEN and RESEX fits to the same form. The three regression curves are quite similar to each other, with our data regression line falling between the curves from MARSEN and RESEX. In other words, our data show good agreement with the results of other studies when considered as a function of wave age, even when comparisons as a function of wind speed to those same studies showed poor agreement.

It is possible that the empirical fit between C_d and C_p/u_* suffers from self-correlation problems because u_* appears on both sides. Following Perrie and Toulany (1990) and Smith et al. (1992), we estimated the spuriousness introduced by the variability of u_*. Spurious correlation would be ignored if the following conditions are met:

$$\text{var}[\ln(u_*^{-0.578})] \ll \text{var}[\ln(u_*/U_{n10})^2 \times u_*^{-0.578}],$$

$$\text{var}[\ln(u_*)] \ll \text{var}[\ln(C_p)]. \quad (19)$$

For our 119 data points, the estimated variances are $0.0527 < 0.126$ and $0.158 < 0.333$. Both conditions are not strictly met, but are approximately met. This means C_p and u_* have a good range to avoid self-correlation problems in our dataset.

The wave height and steepness dependence of surface roughness proposed by Taylor and Yelland (2001) does not explain our data very well. We calculated the drag coefficient corresponding to Eq. (11) based on measured H_s and wave steepness for comparison to C_d from direct flux measurements. The results are presented in Fig. 7, where it is apparent that Eq. (11) underpredicted C_d severely for young waves ($C_p/u_* < 12$), just as Taylor and Yelland pointed out in their study.

The temporal variability of the drag coefficient in our dataset is illustrated in Fig. 8, where an 11-h time series data segment of nearly continuous estimates of wind and drag coefficient are presented beginning at 0000 EST 23 July 1998. Here U_{n10} increased from less than 2 m s^{-1} to near 8 m s^{-1} in 8 hours with almost the same wind direction from southwest toward the northeast (Fig. 8b). The correlation coefficient between measured H_s and U_{n10} for the whole experiment was 0.78 and the waves followed the wind direction very closely (Lin et al. 2002). The calculated C_d from air–sea flux measurements shows a significantly higher value for low winds than that for higher winds (Fig. 8c). Equation (17) predicted a nearly constant C_d and Eq. (18) un-

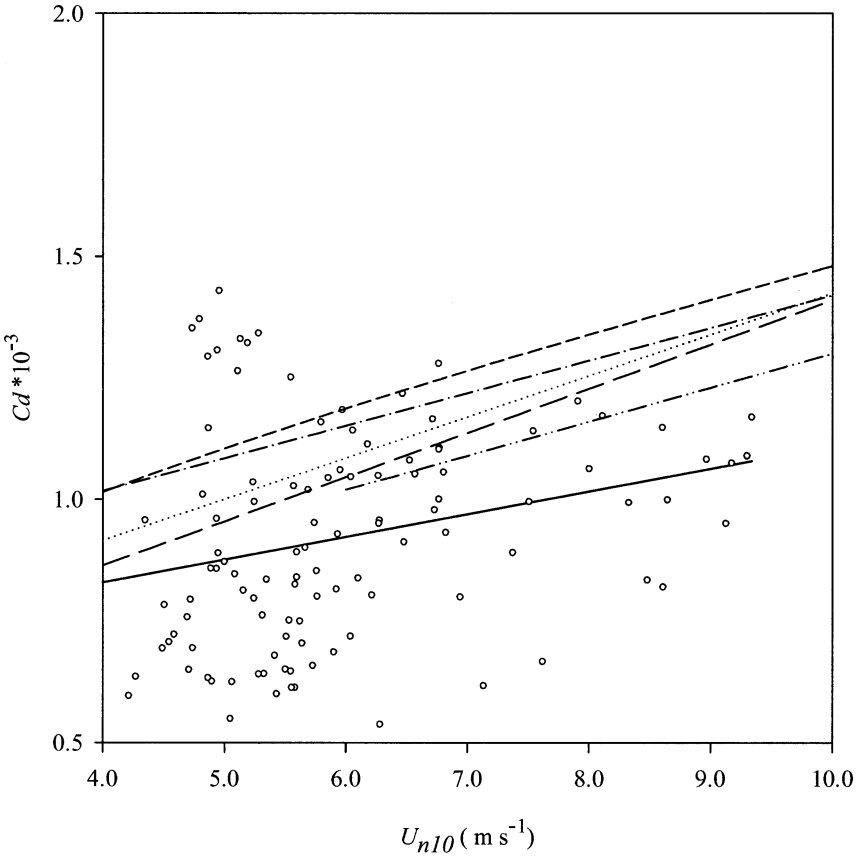

FIG. 5. Linear regression between the measured neutral drag coefficients and the mean wind speeds, U_{n10}, as compared with results from other field studies. Data points are shown by open circles. Lines from the top to the bottom are: Charnock (short dash), RASEX (dash-dotted), MARSEN (dotted), HEXMAX (long-dash), SWADE (dash-dotted-dotted), and regression from data by Eq. (18) (solid).

derpredicted the C_d over the entire period. Equation (9) predicted a C_d in a better agreement with the data. The measured and calculated C_d are further shown as a function of U_{n10} in Fig. 8d. Once again, C_d increases with decreasing wind speed under light winds ($U_{n10} < 4$ m s^{-1}) and has values much higher than for relatively higher wind speeds (4 m s$^{-1} < U_{n10} < 10$ m s^{-1}). The scatter for low winds is significantly larger than for higher winds.

4. Modeling air–sea interaction processes

a. Model description

Numerical models have been used previously to study wave effects on drag. Janssen (1989) used a numerical model based on resonant wave–mean flow interaction and the quasilinear theory of wind wave generation to theoretically study the effects of waves and air turbulence on the wind profile. He found that there is a strong coupling between wind and waves for young windseas and that a C_p/u_* scaling of C_d is better than U_{n10}. However, the iteration procedure to solve the nonlinear set of equations in Janssen's model was too time consuming to apply operationally (Janssen 1991). We used a relatively simple numerical wave model to study the same problem. The model is based on a parametric, deep water numerical wave model first developed by Donelan (1977) and revised by Schwab et al. (1984). The control equation is based on a local momentum balance. The model is time dependent and can accommodate arbitrary wind and geography. Shallow water wave effects are not included, however. The wave energy spectrum $E(f)$ is assumed to follow the JONSWAP spectral shape (Hasselmann et al. 1973). Estimated C_d is output based on the forcing wind speeds and the predicted wave conditions at each hour.

In the wave model, the total drag τ is treated as the sum of a skin friction (or tangential stress) τ_s, and a wave form drag τ_f:τ_s is proportional to U_{n10}^2 as

$$\tau_s = \rho_a C_{ds} U_{n10}^2, \tag{20}$$

where $C_{ds} = 0.7 \times 10^{-3}$ is the skin friction coefficient, and τ_f is assumed to be proportional to the square of the relative velocity between the wind velocity and the wave phase velocity,

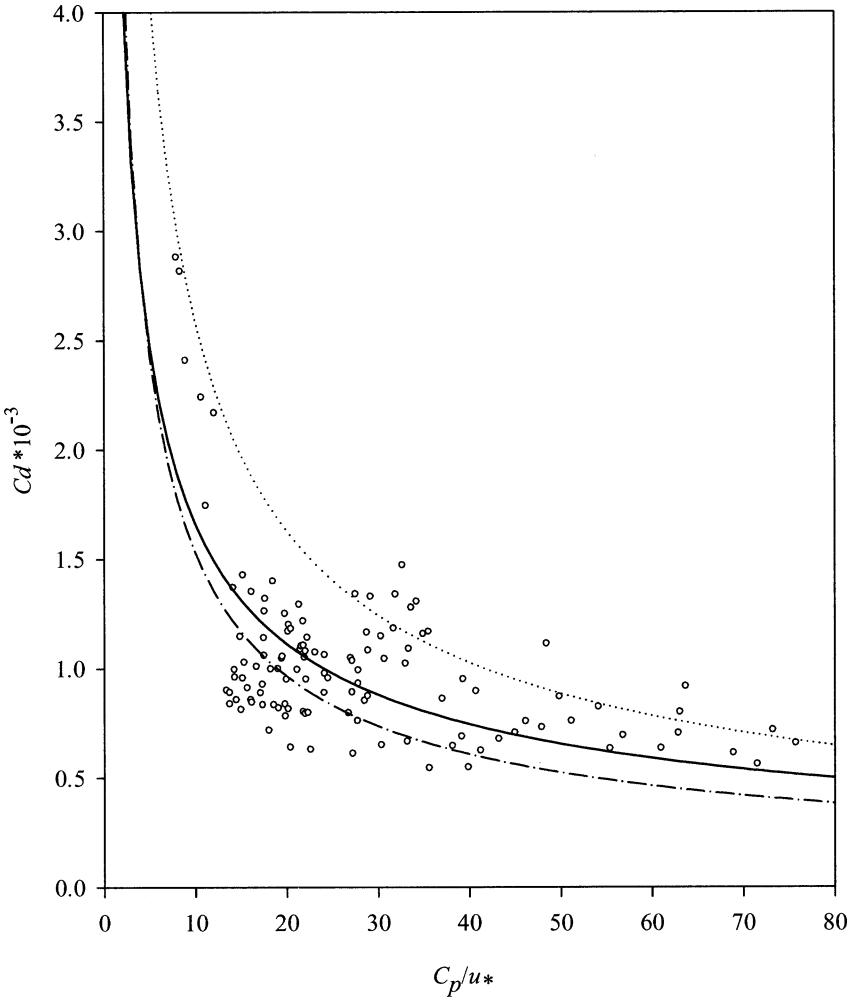

FIG. 6. Nonlinear regression between measured neutral drag coefficient and wave age in Eq. (9). Data points are shown by open circles. Results from the present study (solid line) is in between those from MARSEN (dotted line) and RASEX (dash-dotted line).

$$\tau_f = \rho_a D_f (U_{n10} - C)|U_{n10} - C|. \quad (21)$$

This is similar to the treatment of a mobile sea surface proposed by Kitaigorodskii and Volkov (1965). The wave form drag changes with the development of waves, such that in a fully developed sea the dominant wave travels at a phase speed close to the wind velocity and τ_f becomes smaller and smaller. Full development corresponds to wave age, $C_p/U_{n10} = 1.2$ (Donelan 1990; Pierson and Moskowitz 1964; Bretschneider 1973). A relationship between the mean wave phase velocity C and peak wave phase velocity C_p was proposed by Bretschneider (1973) as $C_p/C = 1.2$. Using this relationship

$$\tau_f = \rho_a D_f (U_{n10} - 0.83C_p) \times |U_{n10} - 0.83C_p|, \quad (22)$$

where D_f is the form drag coefficient given by

$$D_f = \left[\frac{\kappa}{\ln(10/z_0)}\right]^2. \quad (23)$$

In the original model, $z_0 = \sigma/5$ was used where $\sigma^2 = \int_0^\infty E(f)\,df$ is the variance of surface elevation. We tested this expression against the data and found that it predicted values of z_0 one to two orders of magnitude higher than the observed surface roughness. We modified the original model to calculate z_0 using Eq. (10), which explicitly accounts for the effect of wave age on surface roughness and agrees better with our data. Finally C_d is calculated as

$$C_d = \frac{\tau_s + \tau_f}{\rho U_{n10}^2}. \quad (24)$$

b. Application

The modified wave model was run for the experimental period. The geographic region of interest was represented as a horizontal grid covering the area north of 36°39′N, south of 39°36′N, east of 77°23′W and west

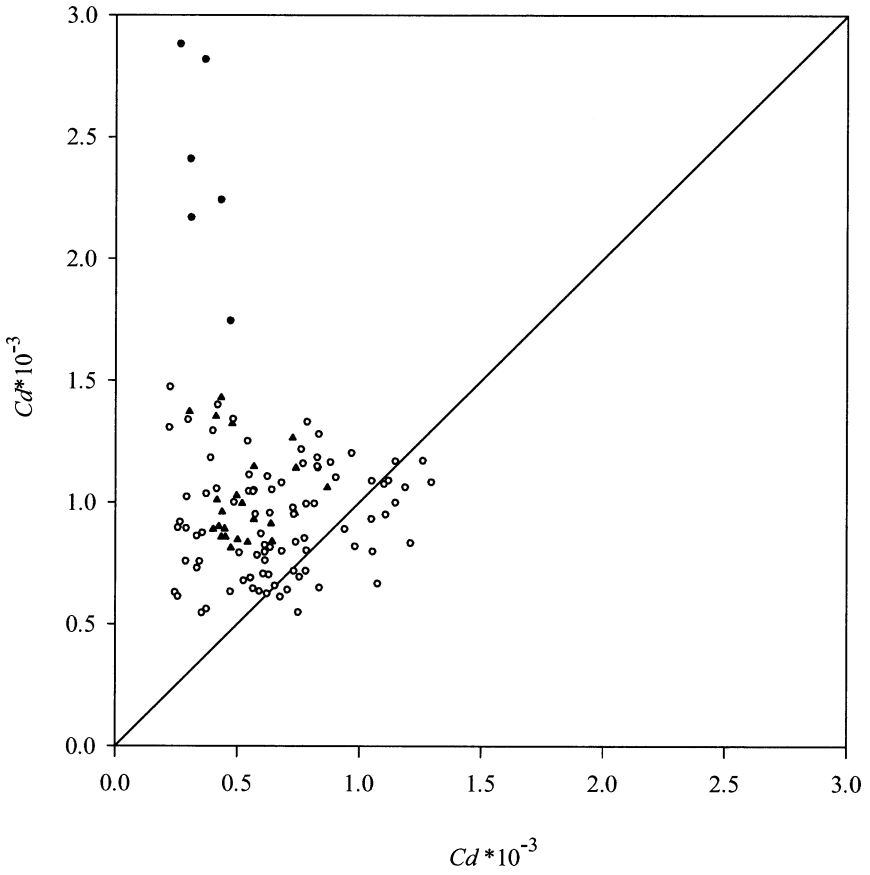

FIG. 7. Comparison of the measured neutral drag coefficients from the flux measurement (y axis) with those calculated by Eq. (11) (x axis) (Taylor and Yelland 2001). Solid circles: $C_p/u_* < 12$, solid triangles: $12 < C_p/u_* < 20$, and open circles: $C_p/u_* > 20$.

of 75°40′30″W. The west–east direction was divided into 410 grid points with a spatial resolution of 365.3 m and a total length of 149.8 km. The south–north direction was divided into 708 grid points with a spatial resolution of 462.5 m and a total length of 327.5 km.

Hourly wind speeds from the CBOS buoy were used along with wind data from the Thomas Point Light (TPL) tower maintained by NOAA. TPL is located at 38°59′18″N, 76°26′12″W, approximately 55 km north of the tower (Fig. 1). Wind speed and direction were measured hourly at $z = 18$ m. Wind speeds were converted to U_{n10} according to the following procedure. An initial guess of u_* is calculated, based on $C_d = 1.2875 \times 10^{-3}$ (Wu 1982), when $U_{n10} < 7.5$ m s^{-1}, and $C_d = (0.8 + 0.065 \times U_{n10}) \times 10^{-3}$ (WAMDI Group 1988), when $U_{n10} \geq 7.5$ m s^{-1}. For this initial guess, U_z is used instead of U_{n10}. The friction velocity u_* is then estimated. If the boundary layer is neutral, the measured wind U_z only needs to be adjusted to 10-m height using similarity theory. If the boundary layer is stable or unstable, then L in Eq. (2) is first calculated without stability correction [assuming $\psi_m(z/L) = 0$]. An iterative process is then started to calculate the stability parameter in Eq. (3) or (4) with the initially estimated L. After L was recalculated in Eq. (2) with the stability correction, the stability parameter in Eqs. (3) or (4) could be recalculated as well. A new u_* was then estimated. This process was repeated until the u_* estimates converged ($\Delta u_* \leq 10^{-6}$). Then U_{n10} was interpolated linearly over latitude for model input. The model determined the time step dynamically based on maximum winds for each hour. The time step ranged from 0.1 to 3 min; H_s, T_p, and C_d were output every hour for further analysis.

c. Results

The model-predicted H_s and T_p are plotted against the measured data in Fig. 9 for measured $H_s \geq 10$ cm (total 129 data points). Figure 9 shows that the wave model predicted H_s and T_p reasonably, though with a fair amount of scatter. The scatter index (SI) is defined as the root-mean-square error normalized by the mean observed value of the reference quantity. It is found that SI = 0.58 for H_s and SI = 0.36 for T_p.

The 220 modeled C_d are grouped into nine 1 m s^{-1} interval wind speed bins. The mean values of C_d, standard deviation, standard error, and the sample number for each wind speed bin are listed in Table 1. Bin-av-

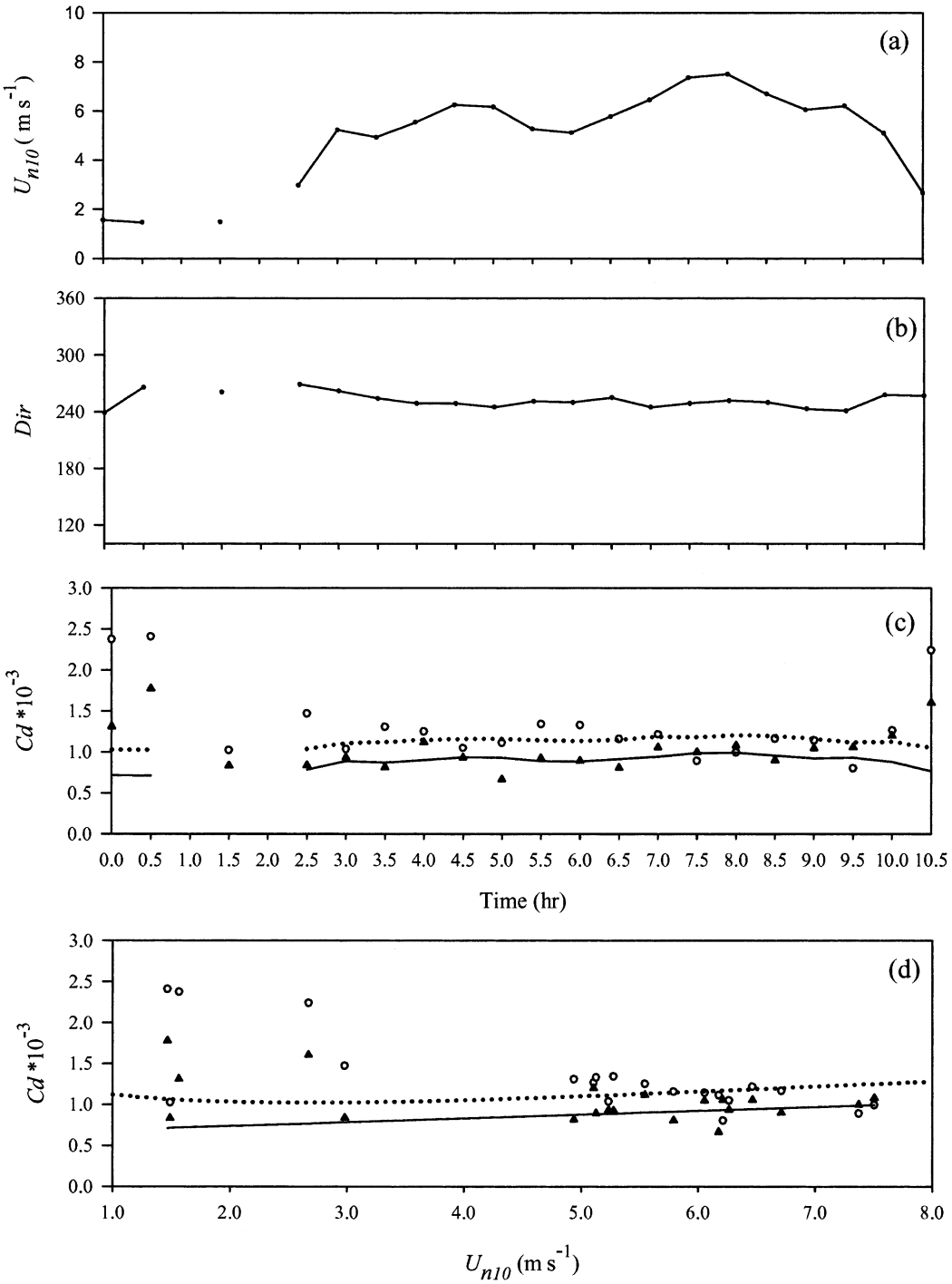

FIG. 8. An 11-h time series of (a) neutral wind speed, (b) wind direction, and (c) the drag coefficients. The C_d in (c) was calculated from flux measurements (open circles), from linear regression in Eq. (18) (solid lines), from the regression with wave age in Eq. (9) (solid triangles), and from Eq. (17) (dotted line). These C_d are plotted against the mean wind speeds U_{n10} in (d).

eraged predicted C_d with standard error bars is also plotted against mean wind speed in Fig. 10 for comparison to the bin-averaged data. In comparison with the data, the model standard errors are significantly smaller, as expected. Similar to the data, however, the standard errors in light winds are much larger than those for higher winds. Modeled C_d increased with decreasing wind speed under light winds ($U_{n10} < 3$ m s^{-1}), with higher

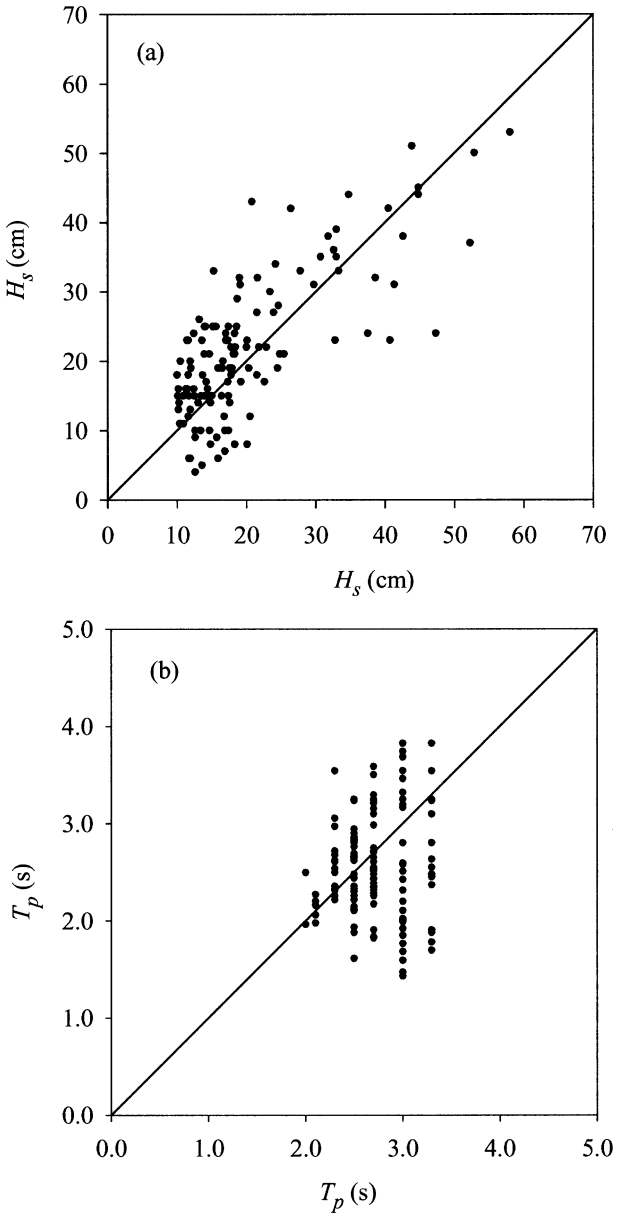

FIG. 9. (a) The wave model–predicted significant wave height H_s (y axis) vs the measured $H_s > 10$ cm (x axis) and (b) the model-predicted peak period T_p (y axis) vs measured T_p (x axis).

values than those at higher winds ($U_{n10} \geq 3$ m s^{-1}). This was the same behavior as the data except that the transitional wind speed from the modeled C_d occurred at $U_{n10} = 3$ m s^{-1} rather than 4 m s^{-1}. Modeled C_d was higher than the data for $U_{n10} \geq 4$ m s^{-1}, but lower for $U_{n10} < 3$ m s^{-1}. Model-predicted C_d was a much better approximation to the data at low wind speeds than any of the other formulations tested, even though the model did not include the effects of increasing viscous sublayer thickness on τ_s.

The 127 modeled data points with $U_{n10} \geq 4$ m s^{-1} are also linearly fit to U_{n10}. The best fit was found to be

$$C_d = (0.0649U_{n10} + 0.699) \times 10^{-3} \qquad (25)$$

with a correlation coefficient of $r = 0.73$, which is significantly larger than that calculated from data. The scatter of the modeled C_d is reduced significantly in comparison to the data, but it is not eliminated. The scatter in H_s and T_p predictions contributes to the scatter of C_d through D_f. The model also predicts 20% higher C_d than that derived directly from the data, and it matches the MARSEN, HEXMAX, and SWADE results.

Model results were also analyzed to fit estimated C_d to estimated wave age using Eq. (9). The best fit gave $A = 6.79 \times 10^{-3}$ and $B = -0.592$, with $r = 0.82$, a standard error for A of 5.606×10^{-4} and for B of 0.027. All of these error indications are significantly smaller than those from the data. The two regression lines from model and data are plotted in Fig. 11 for comparison to the individual model predictions. There is a close agreement between these two lines. The statistical behaviors of the model predictions and the data are very similar when considered as a function of wave age.

d. Discussion

The fact that a relatively simple, momentum-driven deep water wave model did so well at predicting the behavior of the air–sea drag coefficient in Chesapeake Bay is rather remarkable. These predictions were particularly good when considered as a function of wave age, which adds support to the argument that wave age is the dominant control on the air–sea drag coefficient. In a recent laboratory study of the wind stress partition between wave form drag and viscous tangential stress, Banner and Peirson (1998) reported that for wind speed up to 14 m s^{-1} the tangential stress coefficient decreases with wind speed and is relatively insensitive to the sea state. As the overall drag coefficient increases with wind speed, the relative importance of the form drag also increases. According to Fig. 2 in Banner et al. (1999), C_{ds} is in the range of 0.7–0.9 ($\times 10^{-3}$) for $U_{n10} = 6$ m s^{-1} and 0.6–0.8 ($\times 10^{-3}$) for $U_{n10} = 10$ m s^{-1}. In our datasets, the maximum $U_{n10} = 9.34$ m s^{-1}, the constant value of $C_{ds} = 0.7 \times 10^{-3}$ adopted for simplicity in our model (Donelan 1977) is a good approximation in this range.

As observed by Banner and Peirson (1998), the model also predicted an increasing C_d with U_{n10} (see Fig. 10) through the increasing form drag coefficient, D_f with U_{n10}. When waves become fully developed, they no longer contribute to the surface roughness length both because they are not steep and because they travel at speeds equal or higher than the wind speeds (Donelan 1990). When the peak phase speed reaches $1.2U_{n10}$, the wave form drag in Eq. (22) diminishes with D_f being a constant. This means that in a fully developed wave field, the dominant waves traveling at phase speeds close to the wind velocity receive little momentum from air. Since fully developed waves occur in high wind speeds, the stratification effects are not important because $L \propto$

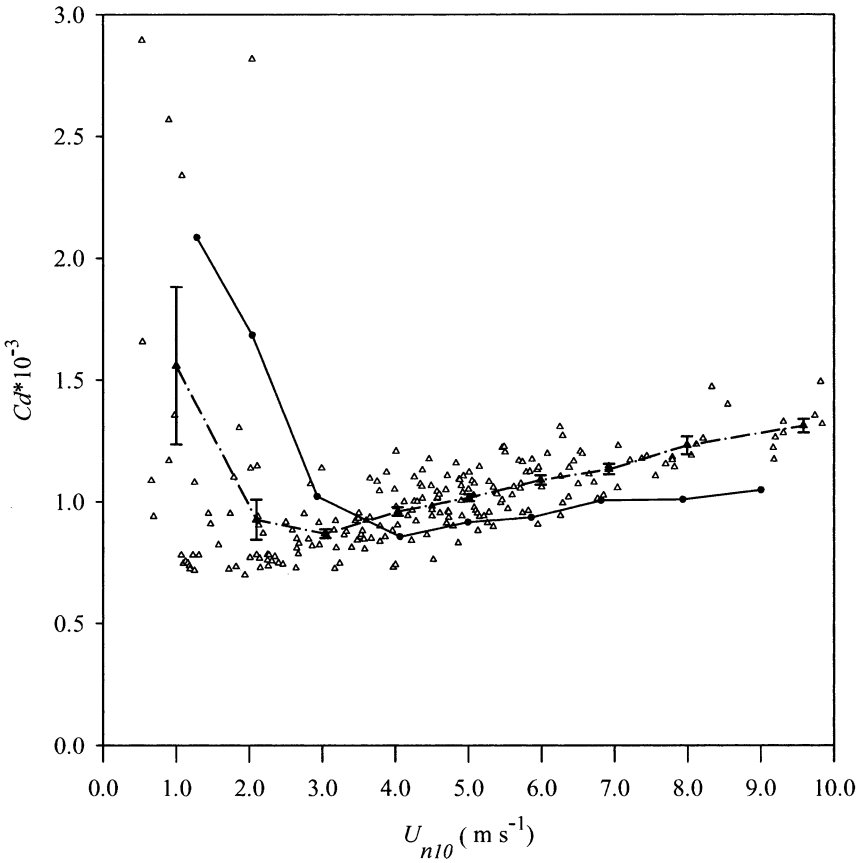

FIG. 10. Comparison of the model-predicted drag coefficients for nine 1 m s^{-1} wind speed bins with the observed mean drag coefficients. Model-predicted C_d are shown by open triangles. The dash-dotted line with solid triangles shows the model-predicted bin-averaged C_d. The error bars represent standard errors for each bin. The bin-averaged data are shown by solid line with solid circles.

u_*^3 becomes large and since $L \to \infty$, $z/L \to 0$, and $\psi_m(0) = 0$. The similarity theory predicts that the atmospheric boundary layer can be assumed neutrally stratified.

5. Summary and conclusions

In this study, we present data from an atmospheric boundary layer and surface wave study in CB under almost purely fetch-limited conditions, with fetches ranging from a few to tens of kilometers. The analyzed tower data provided us an opportunity to examine the properties of the air–sea drag coefficient for fetch-limited wind waves in low wind conditions. The dataset was unique in that it contained simultaneously measured air–sea fluxes, surface wind waves, and surface current data. The data were obtained in a fetch-limited, semienclosed basin dominated by windseas with very little swell. The analyzed results lead to the following conclusions:

The neutral drag coefficients depend upon both wind speed and wave age, but they are better correlated to wave age than wind speed. When $U_{n10} < 4$ m s^{-1}, the neutral drag coefficients are found to increase with decreasing wind speed and have values much higher than for relatively higher wind speeds. When 4 m s$^{-1} \leq U_{n10} < 10$ m s^{-1}, the neutral drag coefficients increase with increasing wind speed. The data show significantly lower drag coefficients in comparison with other datasets. The data scatter is significantly larger in low winds than in high winds. Regardless of the wind speed, the neutral drag coefficients always decrease with increasing wave age. Regression of the neutral drag coefficients with wave age results in a much higher correlation coefficient than regression with wind speed, and the results agree with those of other studies.

We used a sea-state-dependent surface roughness and a reference system moving with the waves in a parametric numerical wave model to predict wave-age-dependent drag coefficients. The model-predicted drag coefficients reproduce the wind speed dependence of the data qualitatively, though predicted drag coefficients at low wind speeds are slightly lower than the data and predicted drag coefficients at high wind speeds are slightly higher than the data. The modeled drag coefficients reproduce the wave age dependence of the data

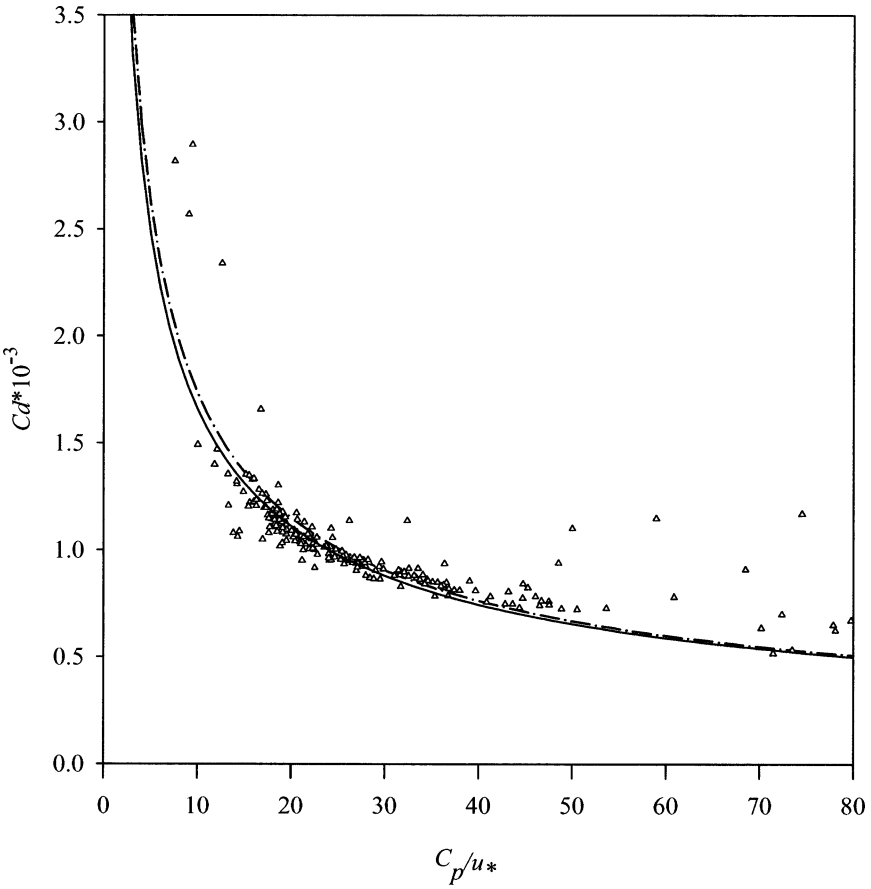

FIG. 11. The regression line calculated from the model-predicted drag coefficients (dash-dotted line) with the model-predicted wave age is compared with that from the measured data (solid line). Model-predicted drag coefficients are shown by open triangles.

very well. This suggests that the momentum transfer mechanism implied by wave-age-dependent drag can be physically explained by a wave-age-dependent form drag coefficient with a dependence on the relative velocity between wind and waves, rather than the absolute wind velocity. The wave model used in this study, which predicts total drag as a byproduct of the wave calculation and is computationally fast, is a good tool for coupling with mesoscale atmospheric models to effect improved, fully coupled estimates of winds, waves, and air–sea fluxes of heat and momentum.

Acknowledgments. We are grateful to Dr. William Boicourt for making space available to us on the tower and for giving us access to the CBOS wind data. We thank Drs. Mark Donelan and David Schwab for sharing their source code and providing guidance on its use. We also thank two anonymous reviewers for their helpful comments. This study was supported by the National Sea Grant Office (Grant NA86RG0037) and by the National Ocean Partnership Program (Grant N00014-98-1-0837).

REFERENCES

Anctil, F., and M. A. Donelan, 1996: Air–water momentum flux observations over shoaling waves. *J. Phys. Oceanogr.,* **26,** 1344–1353.

Ataktürk, S. S., and K. B. Katsaros, 1999: Wind stress and surface waves observed on Lake Washington. *J. Phys. Oceanogr.,* **29,** 633–650.

Baldocchi, D. D., B. B. Hicks, and T. P. Meyers, 1988: Measuring biosphere–atmosphere exchanges of biologically related gases with micro-meteorological methods. *Ecology,* **69,** 1331–1340.

Banner, M. L., and W. L. Peirson, 1998: Tangential stress beneath wind driven air–water interfaces. *J. Fluid Mech.,* **364,** 115–145.

——, W. Chen, E. J. Walsh, J. B. Jensen, S. Lee, and C. Fandry, 1999: The Southern Ocean Waves Experiment. Part I: Overview and mean results. *J. Phys. Oceanogr.,* **29,** 2130–2145.

Boon, J. D., 1998: Wave climate and wave monitoring in lower Chesapeake Bay. *Proc. Third Int. Conf. on Ocean Wave Measurement and Analysis.* Virginia Beach, VA, ASCE, 1076–1087.

Bretschneider, C. L., 1973: Prediction of waves and currents. Look Laboratory Rep., Vol. 3, Honolulu, HI, **3,** 1–17.

Charnock, H., 1955: Wind stress on a water surface. *Quart. J. Roy. Meteor. Soc.,* **81,** 639–640.

——, 1958: A note on empirical wind-wave formulae. *Quart. J. Roy. Meteor. Soc.,* **84,** 443–447.

Chen, W., M. L. Banner, E. J. Walsh, J. B. Jensen, and S. Lee, 2001: The Southern Ocean Waves Experiment. Part II: Sea surface

response to wind speed and wind stress variations. *J. Phys. Oceanogr.*, **31,** 174–198.
Dobson, F. W., and J. A. Elliott, 1978: Wave-pressure correlation measurements over growing sea waves with a wave follower and fixed-height pressure sensors. *Turbulent Fluxes through the Sea Surface, Wave Dynamics, and Prediction*, A. Favre and K. Hasselmann, Eds., Plenum Press, 421–432.
——, S. D. Smith, and R. J. Anderson, 1994: Measuring the relationship between wind stress and sea state in the open ocean in presence of swell. *Atmos.–Ocean*, **32,** 237–256.
Donelan, M. A., 1977: A simple numerical model for wave and wind stress prediction. National Water Research Institute Manuscript, Burlington, ON, Canada, 28 pp.
——, 1990: Air–sea interaction. *The Sea*, B. LeMehaute and D. M. Hanes, Eds., Ocean Engineering Science, Vol. 9, Wiley and Sons, 239–292.
——, J. Hamilton, and W. H. Hui, 1985: Directional spectra of wind-generated waves. *Philos. Trans. Roy. Soc. London*, **A315,** 509–562.
Drennan, W. M., H. C. Graber, and M. A. Donelan, 1999: Evidence for the effects of swell and unsteady winds on marine wind stress. *J. Phys. Oceanogr.*, **29,** 1853–1864.
Erickson, D. J., 1993: A stability dependent theory for air–sea exchange. *J. Geophys. Res.*, **98,** 8417–8488.
Garratt, J. R., 1977: Review of drag coefficients over oceans and continents. *Mon. Wea. Rev.*, **105,** 915–929.
Geernaert, G. L., 1990: Bulk parameterizations for the wind stress and heat fluxes. *Surface Waves and Fluxes.* Vol. 1, *Current Theory*, G. L. Geernaert and W. J. Plant, Eds., Kluwer Academic, 91–172.
——, S. E. Larsen, and F. Hansen, 1987: Measurements of the wind stress, heat flux, and turbulence intensity during storm conditions over the North Sea. *J. Geophys. Res.*, **92,** 13 127–13 139.
——, K. L. Davidson, S. E. Larsen, and T. Mikkelsen, 1988: Wind stress measurements during the tower ocean wave and radar dependence experiment. *J. Geophys. Res.*, **93,** 13 913–13 923.
Hasselmann, K., and Coauthors, 1973: Measurement of wind–wave growth and swell decay during the Joint North Sea Wave Project (JONSWAP). *Dtsch. Hydrogr. Z.*, **12** (Suppl.), A8.
——, J. Bösenberg, M. Dunckel, K. Richter, M. Grünewald, and H. Carlson, 1986: Measurements of wave-induced pressure over surface gravity waves. *Wave Dynamics and Radio Probing of the Ocean Surface*, O. M. Phillips and K. Hasselmann, Eds., Plenum Press, 353–368.
Hsiao, S. V., and O. H. Shemdin, 1983: Measurements of wind velocity and pressure with a wave follower during MARSEN. *J. Geophys. Res.*, **88,** 9841–9849.
Hsu, S. A., 1974: A dynamic roughness equation and its application to wind stress determination at the air–sea interface. *J. Phys. Oceanogr.*, **4,** 116–120.
Janssen, P. A. E. M., 1989: Wave-induced stress and the drag of air flow over sea waves. *J. Phys. Oceanogr.*, **19,** 745–754.
——, 1991: Quasi-linear theory of wind wave generation applied to wave forecasting. *J. Phys. Oceanogr.*, **21,** 1631–1642.
Kitaigorodskii, S. A., 1968: On the calculation of the aerodynamic roughness of the sea surface. *Bull. Acad. Sci. USSR, Atmos. Oceanic Phys.*, **4,** 498–512.
——, 1970: *The Physics of Air–Sea Interaction.* Israel Program for Scientific Translations, 273 pp.
——, and Y. A. Volkov, 1965: On the roughness parameter of the sea surface and the calculation of momentum flux in the near-water layer of the atmosphere. *Izv. Atmos. Oceanic Phys.*, **1,** 973–988.
Large, W. G., and S. Pond, 1981: Open ocean momentum flux measurements in moderate to strong winds. *J. Phys. Oceanogr.*, **11,** 324–336.
——, and ——, 1982: Sensible and latent heat flux measurements over the ocean. *J. Phys. Oceanogr.*, **12,** 464–482.
Lin, W., 2000: Modeling surface wind waves and their effects on air–sea fluxes in Chesapeake Bay. Ph.D. dissertation, University of Maryland Center for Environmental Science, Cambridge, MD, 226 pp.
——, L. P. Sanford, B. J. Alleva, and D. J. Schwab, 1998: Surface wind wave modeling in Chesapeake Bay. *Proc. Third Int. Conf. on Ocean Wave Measurement and Analysis*. Virginia Beach, VA, ASCE, 1048–1062.
——, ——, and S. E. Suttles, 2002: Wave measurement and modeling in Chesapeake Bay. *Cont. Shelf Res.*, in press.
Liu, W. T., K. B. Katsaros, and J. A. Businger, 1979: Bulk parameterizations of air–sea exchanges of heat and water vapor including the molecular constraints at the interface. *J. Atmos. Sci.*, **36,** 1722–1735.
Longuet-Higgins, M. S., D. E. Cartwright, and N. D. Smith, 1963: Observations of the directional spectrum of sea waves using the motions of a floating buoy. *Ocean Wave Spectra*, Prentice Hall, 111–132.
Mahrt, L., D. Vicks, J. Howell, J. Højstrup, J. M. Wilczak, J. Edson, and J. Hare, 1996: Sea surface drag coefficients in the Risø Air Sea Experiment. *J. Geophys. Res.*, **101,** 14 327–14 335.
McMillan, R. T., 1987: An eddy correlation technique with extended application to non-simple terrain. *Bound.-Layer Meteor.*, **43,** 231–245.
Merzi, N., and W. H. Graf, 1985: Evaluation of the drag coefficient considering the effects of mobility of the roughness elements. *Ann. Geophys.*, **3,** 473–478.
Monin, A. S., and A. M. Obukhov, 1954: Basic laws of turbulent mixing in the atmosphere near the ground. *Tr. Geofiz. Inst., Akad. Nauk SSSR*, **24,** 163–187.
Nielsen, P., 1989: Analysis of natural waves by local approximations. *J. Waterw. Port Coastal Ocean Eng.*, **115,** 384–396.
Panofsky, H. A., and J. A. Dutton, 1984: *Atmospheric Turbulence: Models and Methods for Engineering Applications.* John Wiley Intersciences, 397 pp.
Perrie, W., and B. Toulany, 1990: Fetch relations for wind-generated waves as a function of wind stress scaling. *J. Phys. Oceanogr.*, **20,** 1666–1681.
Pierson, W. J., 1983: The measurement of the synoptic scale wind over the ocean. *J. Geophys. Res.*, **88,** 1683–1708.
——, and L. Moskowitz, 1964: A proposed spectral form for fully developed wind seas based on the similarity theory of S. A. Kitaigorodskii. *J. Geophys. Res.*, **69,** 5181–5190.
Rieder, K. F., 1997: Analysis of sea-surface drag parameterizations in open ocean conditions. *Bound.-Layer Meteor.*, **82,** 355–377.
Sanford, L. P., 1994: Wave forced resuspension of upper Chesapeake muds. *Estuaries*, **17,** 148–165.
Schwab, D. J., J. R. Benett, P. C. Liu, and M. A. Donelan, 1984: Application of a simple numerical wave prediction model to Lake Erie. *J. Geophys. Res.*, **89,** 3586–3592.
Smith, S. D., 1980: Wind stress and heat flux over the ocean in gale force winds. *J. Phys. Oceanogr.*, **10,** 709–726.
——, 1988: Coefficients for sea surface wind stress, heat flux, and wind profiles as a function of wind speed and temperature. *J. Geophys. Res.*, **93,** 15 467–15 472.
——, and E. G. Banke, 1975: Variation of the sea surface drag coefficient with wind speed. *Quart. J. Roy. Meteor. Soc.*, **101,** 665–673.
——, and Coauthors, 1992: Sea surface wind stress and drag coefficients: The HEXOS results. *Bound.-Layer Meteor.*, **60,** 109–142.
Snyder, R. L., F. W. Dobson, J. A. Elliott, and R. B. Long, 1981: Array measurements of atmospheric pressure fluctuations above surface gravity waves. *J. Fluid Mech.*, **102,** 1–59.
Stewart, R. W., 1974: The air–sea momentum exchange. *Bound.-Layer Meteor.*, **6,** 151–167.
Taylor, P. K., and M. J. Yelland, 2001: The dependence of sea surface roughness on the height and steepness of the waves. *J. Phys. Oceanogr.*, **31,** 572–590.
Toba, Y., N. Iida, H. Kawamura, N. Ebuchi, and I. S. F. Jones, 1990:

Wave dependence of sea-surface wind stress. *J. Phys. Oceanogr.*, **20,** 705–721.
Valigura, R. A., 1995: Iterative bulk exchange model for estimating air–water transfer of HNO_3. *J. Geophys. Res.*, **100,** 26 045–26 050.
Vickers, D., and L. Mahrt, 1997: Fetch limited drag coefficients. *Bound.-Layer Meteor.*, **85,** 53–79.
WAMDI Group, 1988: The WAM model—a third generation ocean wave prediction model. *J. Phys. Oceanogr.*, **18,** 1775–1810.
Wu, J., 1980: Wind stress coefficients over the sea surface near neutral conditions—A revisit. *J. Phys. Oceanogr.*, **10,** 727–740.
——, 1982: Wind-stress coefficients over sea surface from breeze to hurricane. *J. Geophys. Res.*, **87,** 9704–9706.